IL NUOVO CIMENTO **44 C** (2021) 13
DOI 10.1393/ncc/i2021-21013-x

COMMUNICATIONS: SIF Congress 2020

Improving data analysis for size-segregated atmospheric aerosol samples

F. CROVA(1)(2)(*) on behalf of V. BERNARDONI(1)(2), A. C. FORELLO(1)(2), S. VALENTINI(1)(2), G. VALLI(1)(2) and R. VECCHI(1)(2)

(1) *Department of Physics, Università degli Studi di Milano - Milan, Italy*
(2) *National Institute of Nuclear Physics, INFN-Milan - Milan, Italy*

received 28 January 2021

Summary. — Size-segregated atmospheric aerosol samples collected with cascade impactors can provide valuable information for the study of aerosol emission sources and processes, especially when size distributions of chemical compounds are retrieved. Nevertheless, such data are rare in the literature and, when available, they are often presented as discrete size distributions since data analysis is not straightforward, thus preventing to retrieve detailed modal structure information. For this reason, all the main steps for a robust analysis of size-segregated data are illustrated in this paper. The `MICRON` code was used to perform data inversion and a sensitivity test on the main input parameters (weights, smoothing parameter, and derivative order) was carried out to investigate how the output is affected by their variations. A method to fit the inverted distribution with log-normal functions and to validate the final output has been implemented and discussed through a case-study.

1. – Introduction

Among the most significant atmospheric components, the scientific community is increasingly interested in the study of atmospheric aerosol, that is the complex system formed by solid and liquid particles suspended in the atmosphere. Indeed, it has an impact on the environment at global and local scale, playing a relevant role in Earth radiative forcing, cloud formation (*e.g.*, [1]), air quality degradation, and visibility impairment (*e.g.*, [2]); moreover, atmospheric aerosol particles can be inhaled by humans causing hazardous effects on health (*e.g.*, [3]).

Aerosol particles are originated by a huge variety of sources and processes (natural or anthropogenic); they can be emitted directly into the atmosphere (primary aerosol) or are formed by gas-to-particle transformation (secondary aerosol). Their size spans over 4–5 orders of magnitude (from few nm to tens of μm) and their physical-chemical

(*) Corresponding author. E-mail: `federica.crova@unimi.it`

properties widely differ in function of particle size. Indeed, aerosol composition, emission sources, and particle size are strongly inter-connected. Typically, aerosol particle size distribution is composed of different modes. The Aitken mode (0.01–0.1 μm) is often found in aerosol particles emitted near fresh combustion processes at high temperature and contributes little to the mass concentration distribution, because Aitken particles rapidly coagulate with each other or with other particles, ending up in the accumulation mode (0.1–1 μm) [4]. Indeed, the main sources of particles in the accumulation mode are related to aged combustion processes and condensation of gases and vapors onto existing particles. When the relative humidity in the atmosphere is high (over 80%), the accumulation mode consists of two overlapping submodes, *i.e.*, the condensation mode (0.2–0.3 μm) and the droplet mode (0.5–0.8 μm) [5]; particles in the droplet mode are originated by the cloud or fog processing of hygroscopic particles in the condensation mode. Supermicron particles are usually found in the coarse mode (2–10 μm) and are formed by mechanical abrasion (*e.g.*, erosion of crustal material, abrasion of vehicle components) and resuspension processes (*e.g.*, soil, road dust, sea spray, pollens). In some cases —*e.g.*, at urban sites— an additional intermediate mode (1–2 μm) can be observed; it has been associated with crustal material, road dust, coal combustion, and regional aerosol, but more research is needed to properly identify the processes associated to this mode [6]. Therefore, size distributions of aerosol chemical species are key information to gain a detailed knowledge of aerosol emission sources and the processes they are involved in (transformation/transport/deposition) (see, *e.g.*, [7]).

Size-segregated aerosol characterisation can be obtained by using cascade impactors (in the following also referred to as multistage impactors); these instruments collect aerosol in different size classes onto suitable supports which can be analysed off-line to retrieve aerosol chemical composition as a function of particle size. Unfortunately, such studies are quite scarce in the literature due to several issues to overcome to provide robust results; indeed, size-fractionated samples are characterised by very small quantities of particulate matter (tens of μg), field campaigns consist in a wide number of samples to be analysed, sampling methods are not automatic and require a huge amount of manpower, analytical methods must be optimized to deal with these small samples, data analysis is time-consuming being not straightforward. It is noteworthy that raw concentration data obtained using cascade impactors do not provide the aerosol population modal structure unless a proper post-processing data analysis is carried out; nevertheless, in the literature often discrete size-segregated functions are reported and assimilated to modal distributions.

In this work, a method for the determination of robust atmospheric aerosol size distributions is presented through an application to experimental data retrieved in a field campaign in Milan (Italy) in winter 2019/2020 by using the multistage impactor SDI (Small Deposit area Impactor, Dekati [8]). In particular, elemental concentration data will be exploited to 1) perform data inversion by using the `MICRON` code [9]; 2) understand how the continuous size distribution output is affected by variations of input parameters; 3) implement a method for fitting the continuous size distribution with a sum of log-normal functions to retrieve modal structure information; 4) validate the final fitting by reconstructing the discrete data and by comparing them to measured ones.

2. – Methodology

2˙1. *Discrete size distribution.* – The operation mode of a cascade impactor is based on the principle of inertial impaction. Briefly, ambient air is accelerated and forced to

pass through a nozzle by using an aspiration pump; the exit stream is directed against an impaction plate so that air streamlines are rapidly deflected and turn around the plate. This system is characterised by a dimension called cut-off diameter ($d_{cut\text{-}off}$) [4]. Aerosol particles having an aerodynamic diameter d_{ae} (*i.e.*, the equivalent diameter of a spherical particle with unitary density $1000\,\mathrm{kg/m^3}$ which has the same inertial properties of the real particle) larger than $d_{cut\text{-}off}$ cannot follow the streamlines and collide with the plate; they are thus removed from the flow and collected onto a suitable support placed onto the plate for off-line analysis. Conversely, smaller particles pass over the plate. In a cascade impactor, a certain number of consecutive impaction plates characterised by decreasing cut-off diameters are placed in series so that aerosol particles pass from one stage to the following, with a resulting particle sampling in discrete size ranges. For an ideal impactor, the cut-off efficiency curve is a step function, *i.e.*, 100% for particles having $d_{ae} > d_{cut\text{-}off}$ and 0% for remaining particles. Nevertheless, in real conditions, some oversize particles can pass through the stage (*e.g.*, because particles can bounce on the collection plate) while undersize particles can be collected (*e.g.*, because of their Brownian motion): the real cut-off curve is therefore less sharp than the ideal one and has to be determined by experimental calibration. Conventionally, it is used to refer to this diameter as the effective cut-off diameter (ECD), which is the diameter for which particles are collected with an efficiency of 50%. Hence, each stage of a multistage impactor is associated with an experimentally determined cut-off efficiency curve. The multistage impactor SDI used in this work consists of 12 stages with ECDs in the range 0.048–8.57 μm; fig. 1 shows the 12 experimental cut-off efficiency curves [8]. It operates at a flow rate of 11 l/min and a pre-impactor inlet was mounted at the top to cut off particles larger than about $12\,\mu$m.

After the collection of size-segregated aerosol samples, particles collected on different stages can be analysed as for their chemical composition (elements, ions, and carbonaceous components; see *e.g.*, [7, 10-12]) and —less frequently due to the small amount of mass— for retrieving size-segregated mass concentration.

Once species concentrations are measured on each stage, the discrete size distribution can be represented as a histogram constructed by dividing the size range of the collected particles into a series of N discrete intervals —where N is the number of stages— and by assigning to the bar height i the concentration measured on stage i. However, each interval has a different width since ECDs are not equally spaced, thus a normalisation is mandatory to directly compare concentrations in different size intervals. Moreover, as previously stated, aerosol particle size spans over 4–5 orders of magnitude, therefore a clearer representation of the histogram is commonly obtained by representing the diameter axis in logarithmic scale. To take into account these observations, histogram bars are constructed so that the bar width related to the stage i is the logarithmic interval $\Delta\log(d) = \log(ECD_{i+1}/ECD_i)$, while the bar height is the measured concentration ΔC $[\mu\mathrm{g}\cdot\mathrm{m}^{-3}]$ normalised by the bar width: $\Delta C/\Delta\log(d)$ [4]. Ideally, by drawing a smooth curve through the top of the bars, the continuous size distribution expressed as $\mathrm{d}C/\mathrm{d}(\log d)$ could be graphically represented; nevertheless, it is noteworthy that such a distribution would not consider that cut-off efficiency curves are not ideal and can also overlap (see fig. 1); additionally, measurement uncertainties are not taken into account.

2˙2. *Data inversion and fitting.* – To retrieve continuous size distributions, it is therefore necessary to invert the measured data. The inversion is not trivial and a variety of algorithms have been reported for this purpose; among them, one of the most used in

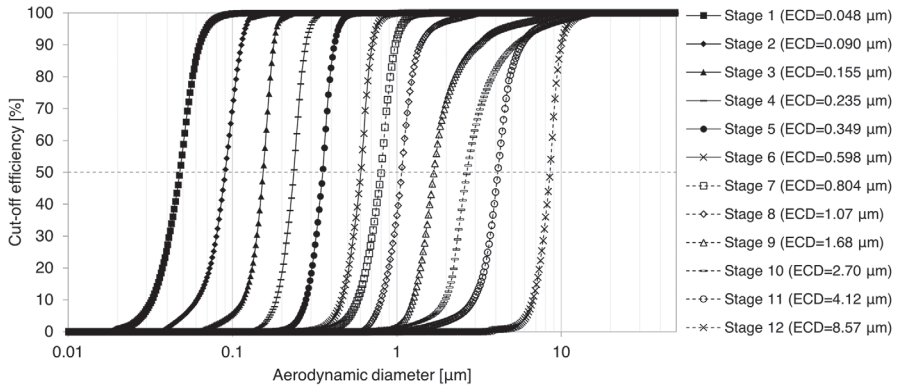

Fig. 1. – Cut-off efficiency curves for the 12 stages of multistage impactor SDI.

the literature is the method implemented in the `MICRON` code (Multi-Instrument inversion using Constrained RegularisatiON [9]) because of its flexibility, as it was not developed for a specific aerosol inversion problem [13]. In the `MICRON` code, the relationship between the measured quantity C_i on the stage i and the continuous size distribution $f(d)$ as a function of the particle diameter d is described by eq. (1):

$$C_i = \int_I K_i(d) f(d) \mathrm{d}d + \epsilon_i, \qquad i = 1, \ldots, N, \tag{1}$$

where $K_i(d)$ is the cut-off efficiency curve for the stage i, N is the number of stages ($N = 12$ for the multistage impactor SDI), I is an interval such that the product $K_i(d)f(d)$ is zero outside this interval and ϵ_i is the modelling residual. This set of integral equations must be inverted for the unknown aerosol size distribution function $f(d)$. However, with only N measured values, at most only N values of $f(d)$ can be exactly determined, and an infinite number of different continuous curves pass through this finite number of points: for this reason, the problem is said to be ill-posed [14]. The algorithm implemented in the `MICRON` code solves this problem by using constrained regularisation to find the size distribution $f(d)$ which best agrees with the measured data. Constrained regularisation consists in the minimisation of a "loss function", that measures the degree of match between the predicted and observed data, to which a regularisation term is added to obtain a smooth distribution $f(d)$, and constraining the solution to non-zero distribution [13]:

$$\min_f \left[\sum_{i=1}^{N} \left(\frac{C_i - \int_I K_i(d) f(d) \, \mathrm{d}d}{E_i} \right)^2 + \lambda \int_I \left(\frac{\mathrm{d}^j f(d)}{\mathrm{d}d^j} \right)^2 \mathrm{d}d \right], \tag{2}$$

where E_i is the user's estimate of ϵ_i, *i.e.*, a weight which at least coincides with analytical uncertainties assigned to measured data, but can be increased to include modelling errors. The regularisation term allows to prevent overfitting; indeed, in the absence of *a priori* information, it is difficult to justify a solution containing structures and oscillations beyond data resolution [9]. This term is expressed as the j-th derivative of $f(d)$ (the choice of j is up to the user) and gives a measure of the smoothness degree of $f(d)$. The weight given to the regularisation term is determined by the smoothing

parameter λ: if λ is too large, the solution will be over-smoothed, while if it is too small, the solution can contain non-existent structures. The algorithm used to determine the smoothing parameter can be chosen among Unconstrained Generalised Cross Validation (called UGCV, or CGCV when non-negativity constraints are taken into account), Unconstrained Ridge Regression (called URR, or CRR when non-negativity constraints are taken into account), and Discrepancy (called DISC); details can be found in [9, 15] and references therein cited. As output, the `MICRON` code gives $f(d)$ reconstructed for a set of diameters (typically about 80 points); moreover, it provides also the reconstructed discrete data, which is a useful tool to check the quality of the inversion procedure.

Once obtained a reliable inversion, the further step is to approximate the output distribution $f(d)$ as a sum of analytical functions to retrieve modal information. In the literature, log-normal functions are typically used for this purpose. Indeed, this distribution empirically matches the observed skewed shapes (long tail at large sizes) of atmospheric aerosol distributions [4]; it has been shown to result from brake-up of large objects into smaller debris or conversely from agglomeration processes [14]; it is characterised by only three parameters (geometric mean aerodynamic diameter d_g, geometric standard deviation σ_g, and modal concentration c); single modes can be easily summed up to provide good fits for the whole distribution of aerosol population; finally, the power of the log-normal distribution resides also on the possibility of calculating (using the Hatch-Choate conversion equations described *e.g.*, in [4]) other moment distribution —as well as their means, medians, and moment averages— when a detailed size distribution is available. In this work, fitting was performed by a script realised on-purpose through the software `MATLAB` [16]. The implemented code is divided into two parts: the first allows to determine a row estimate of d_g [μm], σ_g [μm] and c [$\mu g \cdot m^{-3}$] for each mode (by following the approach described in [17, 18]). The input $f(d)$ distribution is scanned for the maximum value; a number of points n_p specified by the user left and right to the maximum is used for a non-linear least square fit with a log-normal distribution, which is subtracted from input data. The resulting distribution is then scanned again for the new maximum value and a second log-normal is fitted following the same steps. This procedure is iteratively repeated for a number of times M, which corresponds to the number of modes used to fit the original distribution. In the second part of the code, the retrieved parameters are used as input for a second non-linear least square fit, where $f(d)$ is approximated with the sum of the M log-normal distributions. This second step allows refining the determination of log-normal parameters. The number of modes M is fixed by the user; it can be varied to explore which configuration produces modes having physical meaning and reconstructed discrete data as close as possible to the input ones (the method used for data reconstruction will be explained in sect. **3**˙2).

3. – Results and discussion

3˙1. *Optimisation of inversion parameters*. – To better understand how the choices of weights E_i, derivative order j and smoothing parameter λ affect `MICRON` inversion, a sensitivity analysis has been performed. The analysis consisted in keeping fixed two of these parameters at the default values (*i.e.*, $E_i = 10\%$, $j = 3$, URR) and varying the remaining one. The methodology here presented will be shown using potassium (K) as a test element. K has been selected among all the detected elements because its emission processes have been widely studied in the literature, especially at urban sites. Indeed,

the Aitken, condensation, and droplet modes are often found in K distribution in urban environments since K soluble fraction is typically emitted in biomass and residential wood burning ([7,19] and references therein cited). K insoluble fraction is instead found in the coarse mode since it is related both to natural emission such as erosion and resuspension of crustal material, but also to anthropogenic activities such as vehicle-induced resuspension of road dust and mechanical abrasion of vehicle components ([20] and references therein cited). Moreover, some literature works (*e.g.*, [6]) report an additional intermediate mode (1–2 μm) for K at urban sites. All this information was taken into account to determine the set of parameters that produce the most physically reliable outputs in accordance with literature studies and aerosol characteristics.

Firstly, inverted data were retrieved for different sets of weights E_i: 1) analytical uncertainties (for the dataset used in this work, they ranged from a minimum of 6% for the most easily detectable elements in the stages having the highest concentrations, to a maximum of 30% for those elements having low peak to background ratio or low concentrations); 2) uncertainties fixed at 10%; 3) uncertainties fixed at 15%; 4) uncertainties fixed at 20%. In each configuration, for values below minimum detection limits (MDL) an uncertainty equal to 3 times MDL/2 was assigned to significantly underweight them (in accordance with the approach proposed for processing data below MDL *e.g.*, for receptor modelling [21]), while an uncertainty of 20% was assigned to stage 1 and 12, because the measured data in these stages are often not very robust due to experimental issues (*e.g.*, irradiation geometry in the specific case here illustrated). In fig. 2(a), K data inversion is reported; results show that the inverted distributions associated with 15% and 20% uncertainties over-smooth the solution producing only two modes, while those related to analytical and 10% uncertainties are similar and can resolve a more complex structure. To understand which output can be considered more reliable, reconstructed discrete data were compared with input data (fig. 2(b)), revealing that the size distribution associated with analytical and 10% uncertainties reproduce better the measured concentrations. Moreover, distributions related to 15% and 20% uncertainties cannot resolve the Aitken mode at about 0.1 μm, the decomposition of the accumulation mode into the condensation and droplet submodes, and the intermediate mode at about 1.5 μm. The configurations related to analytical and 10% uncertainties resolve also an additional mode at large diameters (about 15 μm) which may be ascribed to large resuspended particles [6], but is outside the experimental size range; then, this information cannot be considered robust since the `MICRON` code extrapolates it, and an additional stage would be necessary to confirm the existence of this mode.

These findings are in accordance with what is reported in other literature works (*e.g.*, [6, 22, 23]) which outline that if uncertainties are set above a certain threshold for several stages (about 10–20% depending on the case), the modal structure becomes broader and it is difficult to distinguish modes close to each other. For all these reasons, analytical uncertainties were chosen as weights for data inversion.

Secondly, inverted data were retrieved by varying the algorithm which determines the smoothing parameter λ. As can be observed in fig. 2(c), the UGCV and the DISC algorithms are not able to produce inverted data in which the intermodal mode is retrieved and the separation of the accumulation mode into the two submodes condensation and droplet is resolved. Moreover, by taking into account the reconstructed *vs.* the input data (fig. 2(d)), the percentage differences associated with the URR algorithm are the lowest for most stages. Therefore, in this application the URR algorithm was chosen for data inversion.

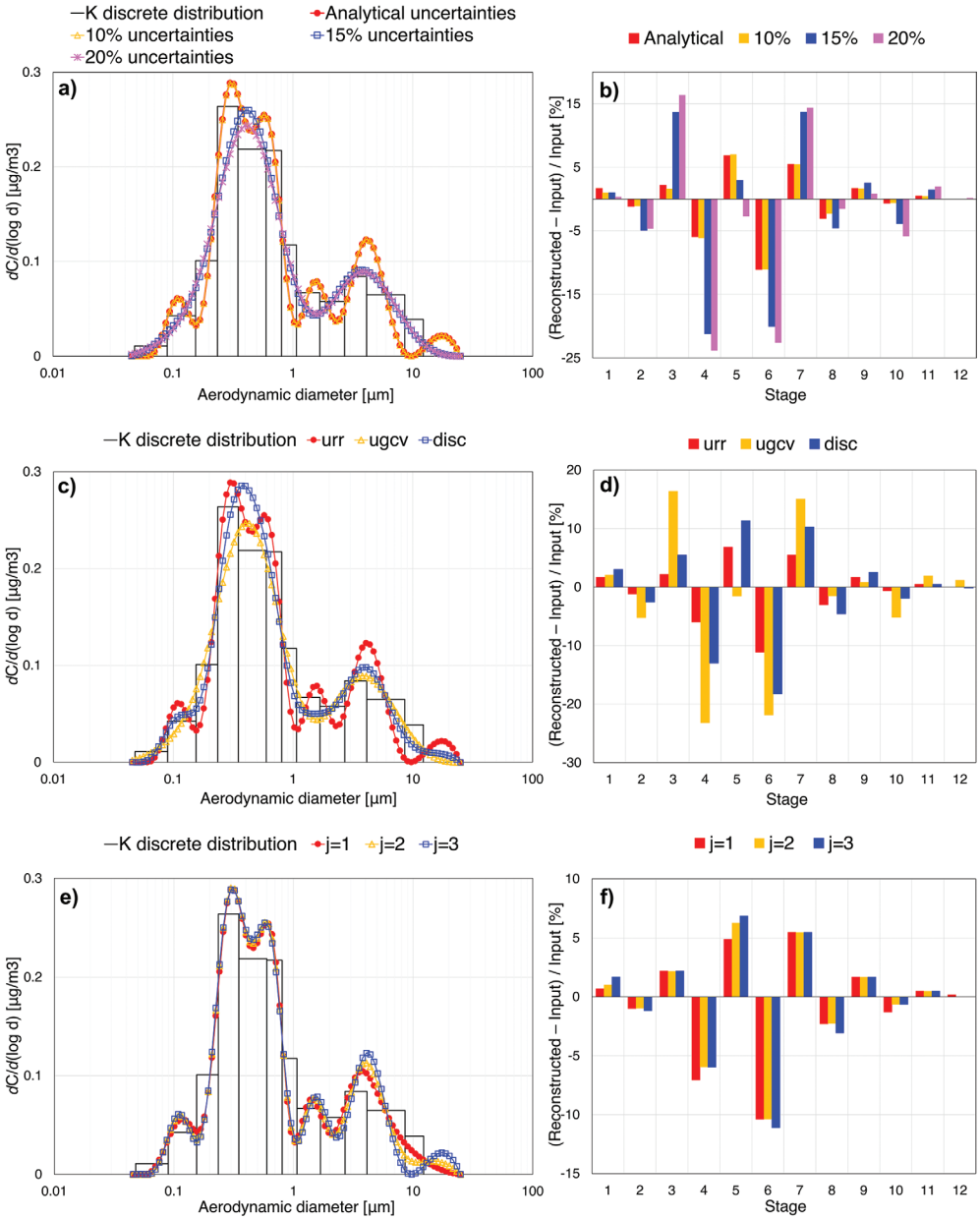

Fig. 2. – Example of sensitivity analysis for potassium (K) data inversion. Panels (a) and (b) show results related to weight tests (weights E_i chosen among analytical, 10%, 15%, and 20% uncertainties); panels (c) and (d) show results related to smoothing parameter tests (smoothing parameter λ chosen among URR, UGCV, and DISC algorithms); panels (e) and (f) show results related to derivative order tests (derivative order j chosen among 1, 2, and 3). In left panels (a), (c), and (e), histograms represent the experimental data, while lines with markers indicate the inverted size distributions $f(d)$ retrieved by `MICRON` for each tested configuration. Right panels (b), (d), and (f) show the plot of percentage differences between input data and reconstructed data for each stage for each tested configuration.

Finally, inverted data were retrieved by varying the derivative order j, which can range from 1 to 5; nevertheless, `MICRON` failed to retrieve the inversion for $j \geq 4$ in all the tested cases. In fig. 2(e) the example of K inverted data is reported; conversely to what was observed in the previous tests, the inversion code can reconstruct the multi-modal structure for each value of j. The inversion in the submicron size fraction is nearly the same for each j, while the main differences can be observed in the coarse mode and the mode at large diameters. The best reconstruction is provided by the configuration with $j = 2$ (fig. 2(f)), for which the percentage differences are the lowest for most stages; however, those related to the other values of j vary less than 1%, therefore there are no significant differences among the three configurations. Considering other elements, the derivative order producing the best reconstructed data varies depending on the element. Comparing the total input mass concentration (*i.e.*, the sum of mass concentration over all the stages) with the total reconstructed sum, it is found that $j = 3$ is the derivative order which allows obtaining the best total reconstructed mass concentration for most elements. Thus, $j = 3$ was chosen as the derivative order for data inversion for this case-study.

3˙2. *Fitting and validation.* – Fitting were performed by exploiting the `MATLAB` code described in sect. **2˙2**. Figure 3(a) shows the fit obtained for K inverted data ($n_p = 4$). Five modes are retrieved: the Aitken mode ($d_g = 0.11\,\mu$m), the condensation mode ($d_g = 0.30\,\mu$m), the droplet mode ($d_g = 0.61\,\mu$m), the intermediate mode ($d_g = 1.57\,\mu$m), and the coarse mode ($d_g = 4.15\,\mu$m). It is worthy to note that the mode at large diameter was not considered reliable for the reasons explained in sect. **3˙1**; however, when fitted, this mode contributes only for about 2% to the total concentration. Thus, it was excluded in the log-normal sum and not showed in the plot. Overall, as also obtained when testing it on the other elements (not shown here for sake of brevity), the implemented code allows to retrieve robust fits and to resolve modes that are close to each other. To evaluate how precisely the final fit represents measured data, a method for the reconstruction of original concentrations on each stage has been implemented in this work. Basically, this method relies on the modelling equation exploited by `MICRON` (eq. (1)) and operates inversely to reconstruct the original data C_i (the reconstructed data will be called R_i in the following). In this case, $f(d)$ is known and coincides with the log-normal sum obtained by the fitting procedure. In eq. (1), the product between $f(d)$ and the cut-off efficiency curve $K_i(d)$ is computed for each stage i and then integrated over the size range. However, efficiency curves are not analytic functions, indeed they are known for a discrete number of diameters d_s (500 points for the curves used in this work); consequently, eq. (1) needs to be discretised. Then, for each stage i and for each diameter d_s, the product $p_i(d_s)$ between $f(d_s)$ and the efficiency cut-off curve $K_i(d_s)$ is computed. In addition, particles collected on the stage i have already passed through the upper stage $i + 1$ with a probability $1 - K_{i+1}$, and similarly for all the following stages up to the last one (*i.e.*, the 12th in the multistage impactor SDI). Thus, to take into account the upper efficiency curves, the product $p_i(d_s)$ [$\mu\mathrm{g} \cdot \mathrm{m}^{-3}$] should be written as

$$(3)\quad p_i(d_s) = K_i(d_s) \cdot \prod_{j=i+1}^{N} [1 - K_j(d_s)] \cdot \sum_{m=1}^{M} \frac{c_m}{\sqrt{2\pi}\log\sigma_{g,m}} \exp\left(\frac{-(\log d_s - \log d_{g,m})^2}{2(\log\sigma_{g,m})^2}\right),$$

where N is the number of stages, M is the number of modes retrieved in the fitting procedure, $d_{g,m}$, $\sigma_{g,m}$, and c_m are, respectively, the mean geometric aerodynamic diameter, the geometric standard deviation and the modal concentration of the m-th mode.

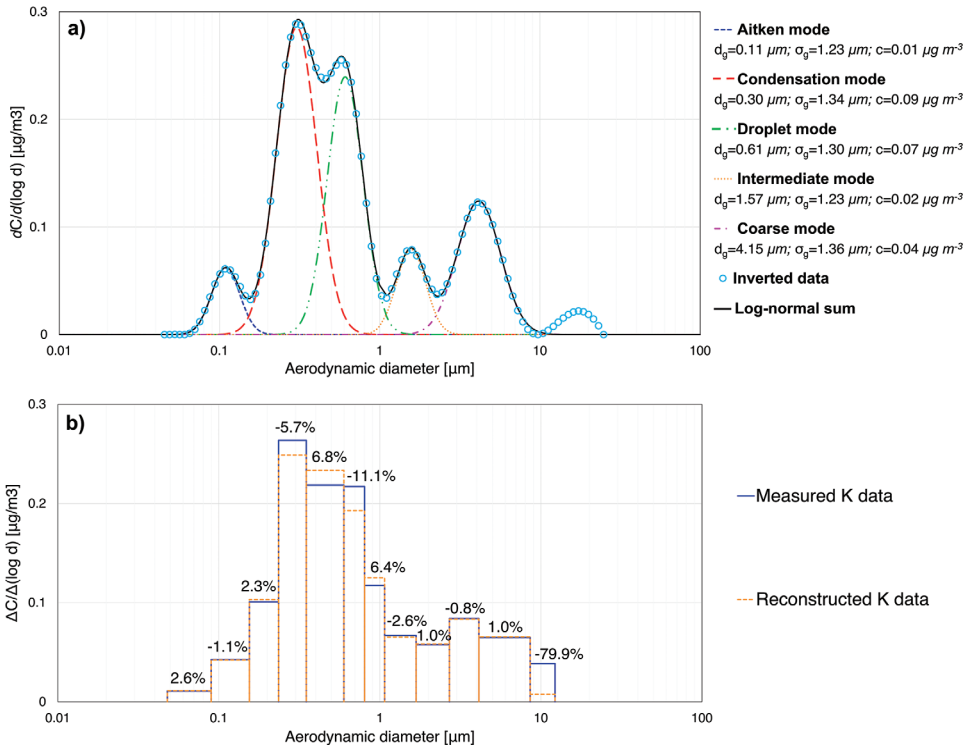

Fig. 3. – (a) Fit of potassium (K) inverted data; geometric mean aerodynamic diameter d_g, geometric standard deviation σ_g, and modal concentration c are reported on the right for each mode in the plot. (b) Reconstructed data R_i *vs.* measured concentration data C_i. Percentage differences $(R_i - C_i)/C_i$ [%] are reported at the top of histogram bars.

The reconstructed concentration R_i on the stage i is thus calculated by approximating the integral in eq. (1) as the discrete sum of $p_i(d_s)$ over the set of d_s. This approximation is computed by multiplying the average between $p_i(d_s)$ and $p_i(d_{s+1})$ for the relative logarithmic interval as follows:

$$R_i = \sum_{s=1}^{S} \left[\left(\frac{p_i(d_s) + p_i(d_{s+1})}{2} \right) \log \left(\frac{d_{s+1}}{d_s} \right) \right]. \tag{4}$$

The reconstruction of K data using as $f(d)$ the log-normal sum previously described (excluding the mode at 17 μm) is presented in fig. 3(b).

4. – Conclusions

In this paper, a detailed methodology for the analysis of size-segregated aerosol samples collected by multistage impactors was presented. Experimental cut-off efficiency curves and measurement uncertainties were taken into account in the inversion of data performed with the `MICRON` code. Analytical uncertainties, $j = 3$, and the URR algorithm were identified by sensitivity tests as those input parameters which optimise the

inversion output in the case taken as example of application. A fitting code based on log-normal distributions was implemented and used for retrieving modal structure information. Besides, a new method for the reconstruction of original data starting from the final fit was applied. Except from the 12th stage (whose reconstruction is not satisfying due to the exclusion of the last mode) most reconstructed data reproduce the measured ones at less than 5%, while in the worst case the percentage difference is 11%. Thus, the inversion and the fitting procedure allows to reconstruct original data with an error comparable to measurement data uncertainties. Moreover, the total mass concentration is reproduced within 2.4%. Similar results are found also for other elements, where total mass concentration is reconstructed at worst within 5%. These findings validate the procedure proposed in this work for the determination of robust atmospheric aerosol size distributions.

* * *

The authors are grateful to prof. Willy Maenhaut for providing the cut-off efficiency curves, the `MICRON` code, and for his useful advices. The authors acknowledge colleagues from ARPA Lombardia and INFN-LABEC for their collaborative work in the field campaign.

REFERENCES

[1] Stocker T. F. *et al.*, *Climate Change 2013: The Physical Science Basis, Contribution of Working Group I to the Fifth Assessment Report of the Intergovernmental Panel on Climate Change*, IPCC Report 2013.
[2] EPA, *Integrated Science Assessment (ISA) For Particulate Matter (Final Report EPA/600/R-08/139F)*, U.S. Environmental Protection Agency Report 2009.
[3] Pope C. A. and Dockery D. W., *J. Air Waste Manag. Assoc.*, **56** (2006) 709.
[4] Hinds W. C., *Aerosol Technology. Properties, Behaviour, and Measurement of Airborne Particles*, 2nd edition (John Wiley & Sons Inc.) 1999.
[5] Seinfeld J. H. and Pandis S. N., *Atmospheric Chemistry and Physics: from Air Pollution to Climate Change*, 2nd edition (John Wiley & Sons Inc.) 2006.
[6] Salma I. *et al.*, *Atmos. Environ.*, **39** (2005) 5363.
[7] Bernardoni V. *et al.*, *Environ. Pollut.*, **231** (2017) 601.
[8] Maenhaut W. *et al.*, *Nucl. Instrum. Methods Phys. Res. B*, **109/110** (1996) 482.
[9] Wolfenbarger K. and Seinfeld J. H., *J. Aerosol Sci.*, **21** (1990) 227.
[10] Bernardoni V. *et al.*, *X-Ray Spectrom.*, **40** (2011) 79.
[11] Calzolai G. *et al.*, *Nucl. Instrum. Methods Phys. Res. B*, **318** (2014) 125.
[12] Viidanoja J. *et al.*, *Aerosol Sci. Technol.*, **36** (2002) 607.
[13] Weber R. J. *et al.*, *J. Aerosol Sci.*, **29** (1998) 601.
[14] Baron P. A. and Willeke K., *Aerosol Measurement, Principles, Techniques, and Applications*, 2nd edition (John Wiley & Sons Inc.) 2005.
[15] Pandis S. N. *et al.*, *J. Aerosol Sci.*, **22** (1991) 417.
[16] MATLAB, Computer Software, version R2020b (The MathWorks Inc., Natick, Mass., US) 2020.
[17] Winklmayr W. *et al.*, *Aerosol Sci. Technol.*, **13** (1990) 322.
[18] Havránek V. *et al.*, *Nucl. Instrum. Methods Phys. Res. B*, **109/110** (1996) 465.
[19] Park S. *et al.*, *Atmos. Environ.*, **73** (2013) 62.
[20] Viana M. *et al.*, *J. Aerosol Sci.*, **39** (2008) 827.
[21] Norris G. *et al.*, *EPA Positive Matrix Factorization (PMF) 5.0 Fundamentals and User Guide (EPA/600/R-14/108)*, U.S. Environmental Protection Agency Report 2014.
[22] Hillamo R. E. *et al.*, *J. Geophys. Res.*, **106** (2001) 27,555.
[23] Kerminen V. *et al.*, *Tellus B Chem. Phys. Meteorol.*, **49** (1997) 159.